Sports Eng (2012) 15:41–52
DOI 10.1007/s12283-012-0084-9

ORIGINAL ARTICLE

# A new technology for resolving the dynamics of a swinging bat

**Kevin King · Jessandra Hough · Ryan McGinnis · N. C. Perkins**

Published online: 3 February 2012


**Abstract** Hitting a major league fastball, with approximately half a second to react, poses one of the greatest challenges in sports. The ability to hit the ball derives from the dynamics of the bat swing which can be measured using video motion capture. However, doing so necessitates swinging the bat within the confines of a motion capture laboratory, often with considerable time and expense. This paper introduces an inexpensive and highly portable measurement method for use right on the field of play to support player training, coaching, rehabilitation, and player-bat fitting. The method employs a highly miniaturized, wireless MEMS inertial measurement unit (IMU) affixed to the knob of the bat. The IMU incorporates three-axis sensing of bat acceleration and angular velocity with a low-power RF transceiver to transmit this data to a host computer. Analysis of this data yields a near-instantaneous and highly resolved summary of three-dimensional bat dynamics. This paper describes this novel technology for use in baseball and softball, presents example results, and reveals new features of bat motion overlooked in previous studies.

**Keywords** Baseball · Softball · Bat dynamics · Inertial sensors · Sports training

## 1 Introduction

The sport of baseball, fondly referred to in the United States as "America's pastime", is also popular in other countries throughout North and South America and in certain Asian and European countries. An exciting part of the game is the likelihood that a batter will hit a baseball traveling at speeds exceeding 145 kph (90 mph) as thrown by a pitcher from 18.4 m (60.5 ft) away. It is often asserted that hitting a major league fastball, with approximately half a second time interval to react, poses one of the greatest challenges in sports. Witness the fact that exceptional batters only hit the ball and make it to base safely 30–40% of the time. Not surprisingly, the ability to hit the ball derives from the underlying physics of the bat swing as well as the physics of the bat/ball interaction, topics that have drawn considerable attention in both the popular and scientific literature.

For example, scientific studies have considered the biomechanics of the swing [1], ball-bat collision [2, 3], the role of bat-ball compliance in that collision [4–6], the precise collision conditions required to hit a home-run [7], and the similarities between swinging a golf club and a bat [8]. The literature most relevant to this study, however, concerns experimental measurements of the bat swing. Technologies used to measure the bat swing include laser-photodiode systems [9] and single [10] and multiple [1, 11] video cameras. These methods have yielded measurements that contribute towards our understanding of the dynamics of the bat.

Koenig et al. [9] employed a vertically oriented array of lasers and photodiodes to measure bat dynamics projected onto the horizontal plane. The lasers were positioned high above home plate (above the batter's head) with companion photodiodes embedded in home plate. The resulting "two-dimensional light curtain" was used to estimate the position and orientation of the bat in the horizontal plane and the associated bat swing speed and time. Attention focused on how the mass distribution of the bat influences bat swing speed. Measurements reveal that bat swing speed

K. King · J. Hough · R. McGinnis · N. C. Perkins (✉)
Mechanical Engineering, University of Michigan,
2350 Hayward Street, Ann Arbor, MI 48109-2125, USA
e-mail: ncp@umich.edu

decreases with increasing moment of inertia of the bat about a vertical axis through the batter's body. More recently, Cross [8] re-evaluated the horizontal dynamics of the bat swing using a single overhead video camera with 20 ms updates (50 Hz frame rate). The measured bat angular velocity and the linear velocity of the bat mass center were employed to deduce the net force and moment imparted to the grip by the batter's hands. Analysis reveals that the moment reverses sign during the swing to prevent the bat from rotating excessively prior to impact.

The measurement techniques of [8, 9] capture the dynamics of the bat projected onto the horizontal plane thereby yielding lower-bound estimates of bat linear and angular velocities and accelerations. By contrast, three-dimensional measurements of a complete swing can be deduced using multiple high-speed video cameras and standard motion capture techniques. To this end, Welch et al. [1] employed a six-camera set-up with reflective markers fixed to both the bat and the batter to capture three-dimensional marker positions with 5 ms updates (200 Hz frame rate). The synchronized motions of the lower limbs, trunk, shoulders, and upper limbs produce a maximum bat speed of 31 m/s among the 39 professional baseball players recruited for their study. Overall, the bat and batter motion data provide a baseline understanding of swing mechanics to support future concepts for player training and rehabilitation. High-speed motion capture was previously employed by Shapiro [11] who analyzed the three-dimensional motion of the bat alone. Two cameras were positioned for imaging the frontal plane of the subject with three markers on the bat. An inverse dynamics model of the bat was also constructed to estimate the net force/moment system imparted to the grip by the subject. Results reveal two distinct stages of bat motion. During the first stage, the bat drops from a near-vertical initial orientation to a near-horizontal orientation. During the second stage, the bat is rapidly accelerated in the hitting zone as evidenced by large bat angular accelerations that peak just prior to impact.

While the experimental studies above successfully identify major features of bat dynamics, the findings are also limited by restrictions imposed by the measurement methods. For instance, methods that project the three-dimensional bat motions onto the horizontal plane, as in [8, 9], cannot resolve motions orthogonal to this plane including those responsible for the initial and near-vertical "drop" of the bat, any "upper cut" or "chop" of the bat at ball impact, and the bat "droop" that defines the actual (non-horizontal) swing plane of the bat. While these features can be successfully resolved using multi-camera motion capture, as in [1, 11], doing so necessitates swinging the bat within the confines of a motion capture laboratory and with considerable expense and time. The expense and the limited availability of motion capture laboratories necessarily restrict this method for targeted, small scale subject studies, not for routine player training, coaching, rehabilitation, or player-bat fitting.

The objective of this paper is twofold. The first objective is to introduce a novel measurement method for the sports of baseball and softball that holds significant promise as an inexpensive and highly portable bat swing analysis system for use right on the field of play. The second objective is to employ this measurement method to reveal new and important features of the bat motion that have been overlooked in prior studies. The method exploits a highly miniaturized, battery-powered, wireless MEMS inertial measurement unit (IMU) affixed to the knob of the bat. The IMU incorporates three-axis sensing of bat acceleration and angular velocity with a low-power RF transceiver to transmit this data to a host computer. This data yields a near-instantaneous and highly resolved analysis of the three-dimensional dynamics of the bat.

The paper opens with a summary of the miniature, wireless IMU and the measurement theory required to analyze three-dimensional bat dynamics. Next data from example swings are presented that reveal: (1) the major phases of bat motion, (2) the three-dimensional position and orientation of the bat, and (3) the critical timing, velocity and acceleration events during the swing. The paper closes by summarizing the contributions made by this study and the potential future uses of this technology.

## 2 Methods

### 2.1 Miniature wireless inertial measurement unit

The wireless IMU illustrated in Fig. 1 measures the six degree-of-freedom (three-dimensional) motion of a baseball/softball bat. This single-board design, which is believed to be the world's smallest wireless IMU, follows a lineage of progressively smaller IMU designs previously employed for the sports of golf [12–14] and bowling [15]. They serve as examples of a more general concept for employing miniature IMU's for sports training [16, 17].

This six-layer board design uses the two surface layers for mounting components, two internal layers for interconnects, one internal layer to provide power, and one internal layer to provide ground. The outer layer illustrated in Fig. 1a is an analog circuit that includes a three-axis MEMS accelerometer, one dual-axis and one single-axis MEMS angular rate gyros, op-amps, and off-chip components for filtering. The opposite face illustrated in Fig. 1b is a digital circuit containing a microprocessor for AD conversion, a low-power RF transceiver, and a small surface mount antenna. The microprocessor performs 12-bit A/D conversion at 1 kHz sampling for all six sensor channels. The device

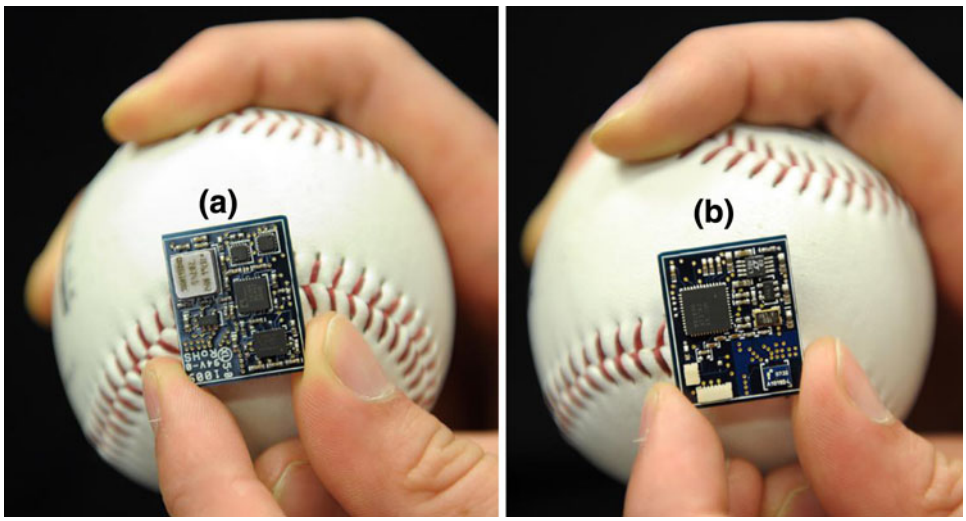


**Fig. 1** Highly miniaturized wireless IMU. **a** analog circuit incorporating MEMS angular rate gyros and accelerometer; **b** digital circuit incorporating microprocessor, wireless transceiver and surface mount antenna

measurement range (and noise floor) includes accelerations up to 18 g's (0.1 mg/$\sqrt{\text{Hz}}$) and angular rates up to 2,000°/s (0.06°/s/$\sqrt{\text{Hz}}$) with an overall measurement bandwidth of 400 Hz. Following transmission, the raw IMU data (acceleration and angular velocity) is low passed filtered using a 100 Hz cut-off frequency to remove measurement noise.

The IMU is calibrated following the method outlined in [18], which identifies both the diagonal and cross-axis sensitivities for the three acceleration axes and the three angular rate axes. The IMU, the battery and a switch are mounted within a small plastic case (Fig. 2a), which is subsequently mounted to the knob end of a bat by a machine screw (Fig. 2b). The assembled board has a footprint of 19 × 22 mm and a mass of 4.5 g (including the mass of a miniature lithium-ion battery) while the fully assembled design in the plastic casing has a mass of 18.9 g which is an extremely small (2%) fraction of the mass of the bat (880 g). The low-power RF transceiver on the IMU can transmit up to 60 ft in low RF, open-air environments. A USB-enabled receiver allows data collection on a host (laptop) computer via custom data collection software. Prior to use, the position of the sweet spot of the bat is measured relative to the accelerometer as required in the measurement theory summarized next.

## 2.2 Overview of measurement theory

The motion of the bat fundamentally reduces to describing the kinematics of a frame of reference fixed to the IMU. This "IMU-frame" is denoted by the triad $(\hat{i},\hat{j},\hat{k})$ in Fig. 3 which is centered at point "$a$", the location of the accelerometer. Moreover, the unit vectors $(\hat{i},\hat{j},\hat{k})$ are aligned with the three sense axes of the accelerometer, which are also aligned with the three sense axes of the angular rate gyros. (The aforementioned calibration procedure detects any cross-axis sensitivities due to small, unintentional misalignments of the accelerometer and rate gyro sense axes). One of these sense axes $(\hat{i})$ is also aligned with the

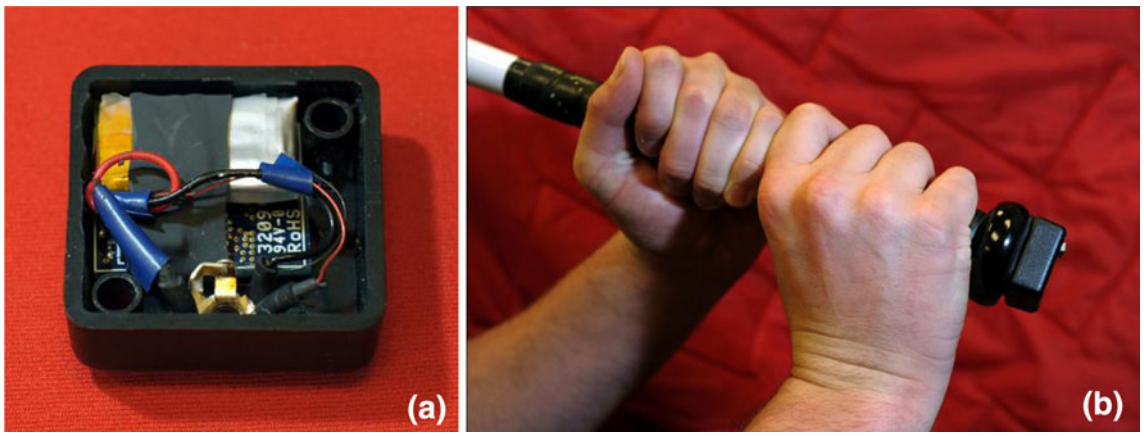


**Fig. 2** **a** IMU is housed in a plastic case that also contains the miniature lithium-ion battery and recharging jack (that doubles as a power switch). **b** The case is mounted to the knob end of the bat using a machine screw


**Fig. 3** IMU-frame $(\hat{i},\hat{j},\hat{k})$ is a bat-fixed frame at the location of the accelerometer (point "$a$") and aligned with the three accelerometer (and rate gyro) sense axes. In addition, $\hat{i}$ is aligned with the bat center-line. Field-frame $(\hat{I},\hat{J},\hat{K})$ is an inertial frame located at the upper left corner of home plate with $\hat{K}$ pointing vertically up and $\hat{J}$ pointing towards the pitcher. Point "$s$" denotes the sweet spot

center-line of the bat, whereas the plane of the remaining two axes $(\hat{i}\times\hat{j})$ coincides with the bat cross-section. Figure 3 also illustrates the "field-frame" defined by the triad $(\hat{I},\hat{J},\hat{K})$. This is an inertial frame of reference located on the upper left corner of home plate with the $\hat{I}\times\hat{J}$ plane defining the horizontal plane of the field ($\hat{I}$ pointing across the plate and $\hat{J}$ pointing toward the pitcher) and $\hat{K}$ pointing vertically up. The point "$s$" denotes the sweet spot of the bat located along the bat center-line near the end.

The direction cosine (rotation) matrix $\underline{C}(t)$ defines the orientation of the sensor frame relative to the field-frame at any time $t$ per

$$\begin{pmatrix}\hat{i}\\ \hat{j}\\ \hat{k}\end{pmatrix} = \underline{C}(t)\begin{pmatrix}\hat{I}\\ \hat{J}\\ \hat{K}\end{pmatrix} \tag{1}$$

The recorded IMU data enables a complete kinematic analysis of the bat motion upon completion of three principal steps:

1. Computation of the direction cosine matrix $\underline{C}(t)$,
2. Computation of $\vec{a}_a(t)$, the acceleration of the point "$a$" in the field (inertial) frame, and the velocity of point of "$a$",
3. Computation of the velocity of point "$s$" (sweet spot) and the bat orientation.

These steps are summarized below.

### 2.2.1 Computation of $\underline{C}(t)$

Begin with computing the direction cosine matrix $\underline{C}(t)$ which can be written in terms of the four Euler parameters $(e_1,e_2,e_3,e_4)$ per [19, 20]

$$\underline{C}(t) = \begin{bmatrix} e_1^2-e_2^2-e_3^2+e_4^2 & 2(e_1e_2+e_3e_4) & 2(e_1e_3-e_2e_4)\\ 2(e_1e_2-e_3e_4) & e_2^2-e_1^2-e_3^2+e_4^2 & 2(e_2e_3+e_1e_4)\\ 2(e_1e_3+e_2e_4) & 2(e_2e_3-e_1e_4) & e_3^2-e_1^2-e_2^2+e_4^2\end{bmatrix} \tag{2}$$

The time-varying Euler parameters are related to the IMU-measured angular velocity

$$\vec{\omega}(t) = \omega_x\hat{i}+\omega_y\hat{j}+\omega_z\hat{k} \tag{3}$$

through the state equations [20, 21]

$$\frac{d}{dt}\begin{pmatrix}e_1\\ e_2\\ e_3\\ e_4\end{pmatrix} = \begin{bmatrix} e_4 & -e_3 & e_2\\ e_3 & e_4 & -e_1\\ -e_2 & e_1 & e_4\\ -e_1 & -e_2 & -e_3\end{bmatrix}\begin{pmatrix}\omega_x\\ \omega_y\\ \omega_z\end{pmatrix} \tag{4}$$

subject to the constraint

$$e_1^2+e_2^2+e_3^2+e_4^2 = 1 \tag{5}$$

Thus, computation of $\underline{C}(t)$ follows immediately from integrating (4), subject to (5), provided initial conditions are given for the Euler parameters.

To this end, consider Fig. 4 which illustrates the initial position and orientation of the bat at the start of a swing trial. Here, the tip of the bat is held at the origin of the field-frame $(\hat{I},\hat{J},\hat{K})$ with the bat center-line held still in the (vertical) $\hat{I}\times\hat{K}$ plane. In other words, the unit vector $\hat{i}$ of the IMU-frame initially lies in the $\hat{I}\times\hat{K}$ plane and forms

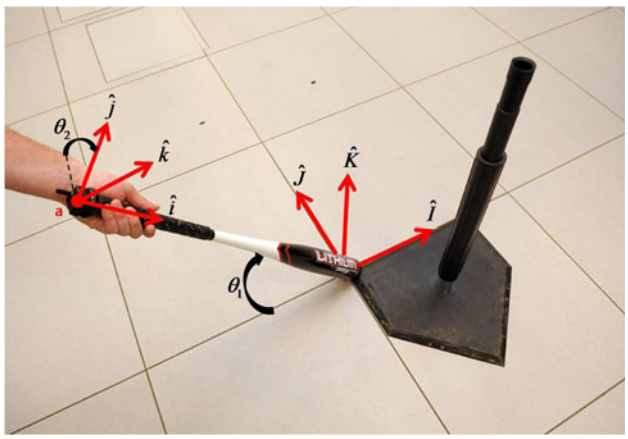


**Fig. 4** The initial bat position and orientation at the start of data collection. The angles $(\theta_1,\theta_2)$ define the initial orientation of the IMU-frame $(\hat{i},\hat{j},\hat{k})$ with the bat center-line $\hat{i}$ held fixed in the vertical $(\hat{I}\times\hat{K})$ plane

the angle $\theta_1$ with the $\hat{I}$ axis as illustrated. The angle $\theta_2$ is a second (roll) rotation about the $\hat{i}$ axis which is also the angle formed between the unit vectors $\hat{j}$and $\hat{J}$. The direction of $\hat{k}$ follows from the right hand rule; $\hat{k} = \hat{i} \times \hat{j}$. Thus, the direction cosine matrix at time $t = 0$ can be written in terms of these two (Euler) angles:

$$\underline{C}(0) = \begin{bmatrix} \cos\theta_1 & 0 & -\sin\theta_1 \\ \sin\theta_1 \sin\theta_2 & \cos\theta_2 & \cos\theta_1 \sin\theta_2 \\ \sin\theta_1 \cos\theta_2 & -\sin\theta_2 & \cos\theta_1 \cos\theta_2 \end{bmatrix} \tag{6}$$

Moreover, one can deduce the two angles $\theta_1$ and $\theta_2$ by exploiting the fact that, when held at rest, the accelerometer measures gravity. In particular,

$$\vec{a}(0) = a_x(0)\hat{i} + a_y(0)\hat{j} + a_z(0)\hat{k} = g\hat{K} \tag{7}$$

Using the definition of $\underline{C}$, Eq. (7) can be re-cast as

$$\begin{aligned} &a_x(0)\hat{i} + a_y(0)\hat{j} + a_z(0)\hat{k} \\ &\quad = g\left[-\sin\theta_1\hat{i} + \cos\theta_1 \sin\theta_2\hat{j} + \cos\theta_1 \cos\theta_2\hat{k}\right] \end{aligned} \tag{8}$$

which yields the solutions

$$\theta_1 = \arcsin[-a_x(0)/g] \tag{9a}$$

$$\theta_2 = \arctan[a_y(0)/a_z(0)] \tag{9b}$$

Upon equating Eq. (2) with Eq. (6) and employing Eq. (9a, b), one can deduce the following initial conditions for the Euler parameters

$$\begin{bmatrix} e_1(0) \\ e_2(0) \\ e_3(0) \\ e_4(0) \end{bmatrix} = \begin{bmatrix} \sin\theta_2(1+\cos\theta_1)/4e_4(0) \\ \sin\theta_1(1+\cos\theta_2)/4e_4(0) \\ -\sin\theta_1 \sin\theta_2/4e_4(0) \\ \sqrt{1+\cos\theta_1+\cos\theta_2+\cos\theta_1\cos\theta_2}/2 \end{bmatrix} \tag{10}$$

### 2.2.2 Computation of $\vec{a}_a(t)$ and $\vec{v}_a(t)$

With $\underline{C}(t)$ now formed at each sampled-instant of time, one can deduce the components of the acceleration of point "$a$" with respect to the field-frame (inertial frame). Let

$$\begin{aligned} \vec{a}_a(t) + g\hat{K} &= a_{ax}\hat{i} + a_{ay}\hat{j} + a_{az}\hat{k} \\ &= A_{ax}\hat{I} + A_{ay}\hat{J} + (A_{az} + g)\hat{K} \end{aligned} \tag{11}$$

in which it is again recognized that the accelerometer at "$a$" measures both the acceleration of "$a$" as well as gravity. Employing the definition of $\underline{C}(t)$ yields

$$\begin{pmatrix} A_{ax}(t) \\ A_{ay}(t) \\ A_{az}(t) \end{pmatrix} = \underline{C}^T(t) \begin{pmatrix} a_{ax}(t) \\ a_{ay}(t) \\ a_{az}(t) \end{pmatrix} - g \begin{pmatrix} 0 \\ 0 \\ 1 \end{pmatrix} \tag{12}$$

Integrating Eq. (12) now provides the velocity of point "a" with components aligned with the field-frame

$$\vec{V}_a(t) = \int_0^t \vec{A}_a(\eta)d\eta \tag{13}$$

where the rest initial condition $\vec{V}_a(0) = 0$ is used.

### 2.2.3 Computation of $\vec{V}_s(t)$ and the bat upper cut, elevation and aim angles

The velocity of the sweet spot "$s$" is an important measure of the bat motion which can be readily deduced from the computed velocity of point "$a$" and the angular velocity of the bat $\vec{\omega}(t)$. Prior to doing so, one must also establish the position of "s" relative to "a"

$$\vec{r}_{s/a} = l\hat{i} \tag{14}$$

where $l$ denotes the (constant) distance from "$a$" to "$s$" along the bat center-line. The velocity of the sweet spot follows from

$$\vec{V}_s(t) = \vec{V}_a(t) + \left[\vec{\omega}(t) \times \vec{r}_{s/a}\right] \tag{15}$$

Note that the latter term, most conveniently written using components in the IMU-frame, can be equivalently written using components in the field-frame by elementary use of (Eq. 1). Doing so provides the desired result

$$\vec{V}_s(t) = V_{sx}(t)\hat{I} + V_{sy}(t)\hat{J} + V_{sz}(t)\hat{K} \tag{16}$$

At least two important "swing metrics" can be deduced from Eq. (16). The magnitude $|\vec{V}_s(t_i)|$ describes the bat "swing speed" developed just prior to impact, at the sampled time $t = t_i$. Moreover, the angle

$$\theta_{\text{upper-cut}} = \arctan\left[V_{sz}(t_i) \Big/ \sqrt{V_{sx}^2(t_i) + V_{sy}^2(t_i)}\right] \tag{17}$$

defines the degree to which the sweet spot is "rising" just prior to impact which is a direct measure of the "upper cut" (angle) of the bat. Conversely, a "chop" follows should the sweet spot be "falling" just prior to impact (i.e., $\theta_{\text{upper-cut}} < 0$).

In addition, the orientation of the bat at impact provides two additional swing metrics. In particular, the bat elevation angle

$$\theta_{\text{elevation}} = \arcsin(C_{13}(t_i)) \tag{18}$$

defines the angle between the bat center-line $(\hat{i})$ and the horizontal $(\hat{I} \times \hat{J})$ plane. Thus, when $\theta_{\text{elevation}} < 0$ (common), the bat has "drooped" below the horizontal at impact. Similarly, the bat aim angle

$$\theta_{\text{aim}} = \arctan[C_{12}(t_i)/C_{11}(t_i)] \tag{19}$$

defines the angle between the bat center-line $(\hat{i})$ and the vertical$(\hat{I} \times \hat{K})$plane at impact. Note that $\theta_{\text{aim}} = 0$ (i.e., bat is parallel to $\hat{I}$ at impact) directs the ball on the line $(\hat{J})$

aimed at the pitcher, whereas $\theta_{\text{aim}} > 0$ (or $\theta_{aim} < 0$) directs the ball to the left (or right) of the pitcher.

## 3 Results and discussion

Experiments were conducted experiments indoors with subjects hitting baseballs off a standard training tee. The tee is integrated into a "home plate" which establishes the location and orientation of the field-frame defined in Fig. 3. Each subject began a trial by first positioning/orienting the bat as defined in Fig. 4, which established the initial conditions for the subsequent swing. Following a command, a subject then "picked-up" the bat from this rest position, executed a normal swing (including impacting the ball), and then returned the bat to the initial (rest) position. During each trial, the IMU wirelessly transmitted acceleration and angular velocity data to a host computer for subsequent analysis per the measurement theory above. The following reports and discusses major findings for example swings and also discusses the possible use of these findings in discriminating batting skill.

### 3.1 Bat orientation, angular velocity and acceleration reveal major phases of bat motion

The direction cosine matrix (Eq. 2) defines the orientation of the IMU-frame as a function of time during the swing. Doing so provides the bat elevation angle (Eq. 18) and aim angle (Eq. 19) at impact as well as at any other time. The elevation and aim angles are two spherical angles that determine the orientation of the bat center-line axis $(\hat{i})$ relative to the field-frame $(\hat{I}, \hat{J}, \hat{K})$. The rotation of the bat about this axis, defined herein as the bat "roll angle", is also readily deduced from components of the direction cosine matrix. Collectively, the bat elevation, aim and roll angles constitute three Euler angles [19] that define the orientation of the IMU-fixed frame relative to the field-frame. The variation of these angles with time reveals the major phases of bat motion.

Consider Fig. 5 which reports the elevation, aim and roll angles computed for an example swing from subject "A". Inspection of these time histories reveals six distinct phases of the motion over a total recording time of 6 s: (1) initial rest ($\approx$0.4 s), (2) backswing ($\approx$1.1 s), (3) set ($\approx$1.1 s), (4) downswing ($\approx$0.165 s), (5) follow through ($\approx$1.8 s), and (6) ending rest ($\approx$1.5 s). At the start of the trial, the subject holds the bat still (refer to Fig. 4) as is readily apparent in the initial "rest" phase where the three angles remain constant. When the swing begins, the subject executes a slow motion "backswing" in which the bat is raised over the subject's shoulder as indicated by the significant increase in the elevation angle to a maximum value. Simultaneously the bat roll and aim angles decrease significantly for the right-handed subject in this example.

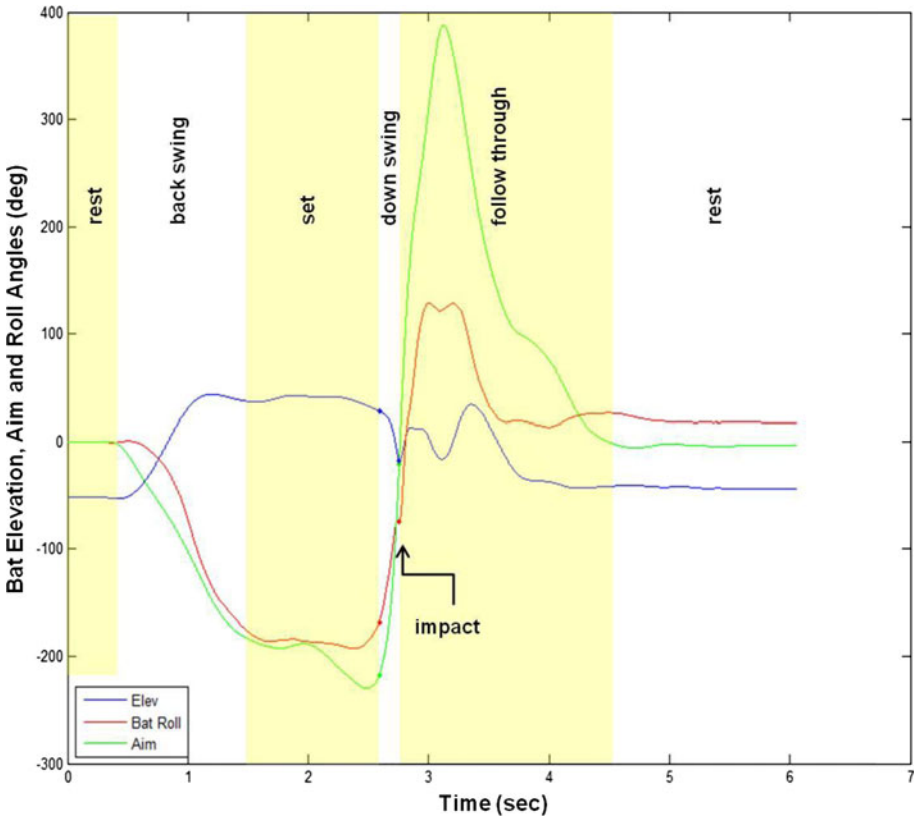


**Fig. 5** Bat elevation, aim and roll angles as functions of time for an example swing by subject A (right-handed). The major phases of the bat motion are readily identifiable

The subject then holds the bat essentially stationary for a short period of time referred to as the "set" position. Some modest bat motion (sometimes referred to as bat "waggle") may also occur during this set phase. Following the set phase, the subject executes a highly dynamic "downswing" marked by a dramatic decrease in the elevation angle and companion increases in the aim and roll angles. The instant of ball impact, denoted in Fig. 5, is clearly evident by the non-smooth transition in any/all of these angles. Following impact, the batter decelerates the bat during the "follow through" and ultimately returns the bat to the final "rest" position where the bat elevation and aim angles return to (approximately) the same values achieved during the initial rest.

These same phases of bat motion are also evident in the "raw" angular velocity and acceleration data recorded as reported in Fig. 6 for the same example. The illustrated time histories of the angular velocity components $(\omega_x, \omega_y, \omega_z)$ and acceleration components $(a_x, a_y, a_z)$ are measured in the IMU-frame and they are low pass filtered with a 100 Hz cut-off. During the initial rest phase, the angular velocity components are zero and the acceleration components sum to $g\hat{K}$. The slow motion backswing produces a smooth transition in angular velocity and acceleration to the near constant values in the set position (where $\vec{\omega} \approx 0$ and $\vec{a}_s \approx g\hat{K}$ except for small but detectable bat waggle). The highly dynamic downswing is readily observable by dramatic increases in the magnitudes of $\vec{\omega}$ and $\vec{a}_s$. The instant of ball impact, denoted in Fig. 6, is clearly evident in the data by near-instantaneous and simultaneous changes in both $\vec{\omega}$ and $\vec{a}_s$ due to abrupt changes in bat linear and angular momenta during impact. Following impact, the batter decelerates the bat during the follow through and ultimately returns the bat to the rest position where $\vec{\omega} = 0$ and $\vec{a}_s = g\hat{K}$ again.

### 3.2 Integration reveals three-dimensional position and orientation of bat

The measurement theory employs the raw data illustrated in Fig. 6 to compute key kinematic measures of the bat swing. For instance, one can readily integrate the velocity of point "$a$" (Eq. 13) to obtain the three-dimensional trajectory traced by the knob end of the bat (hence the trajectory of the batter's hands). At each sampled-time instant, one can then employ the direction cosine matrix

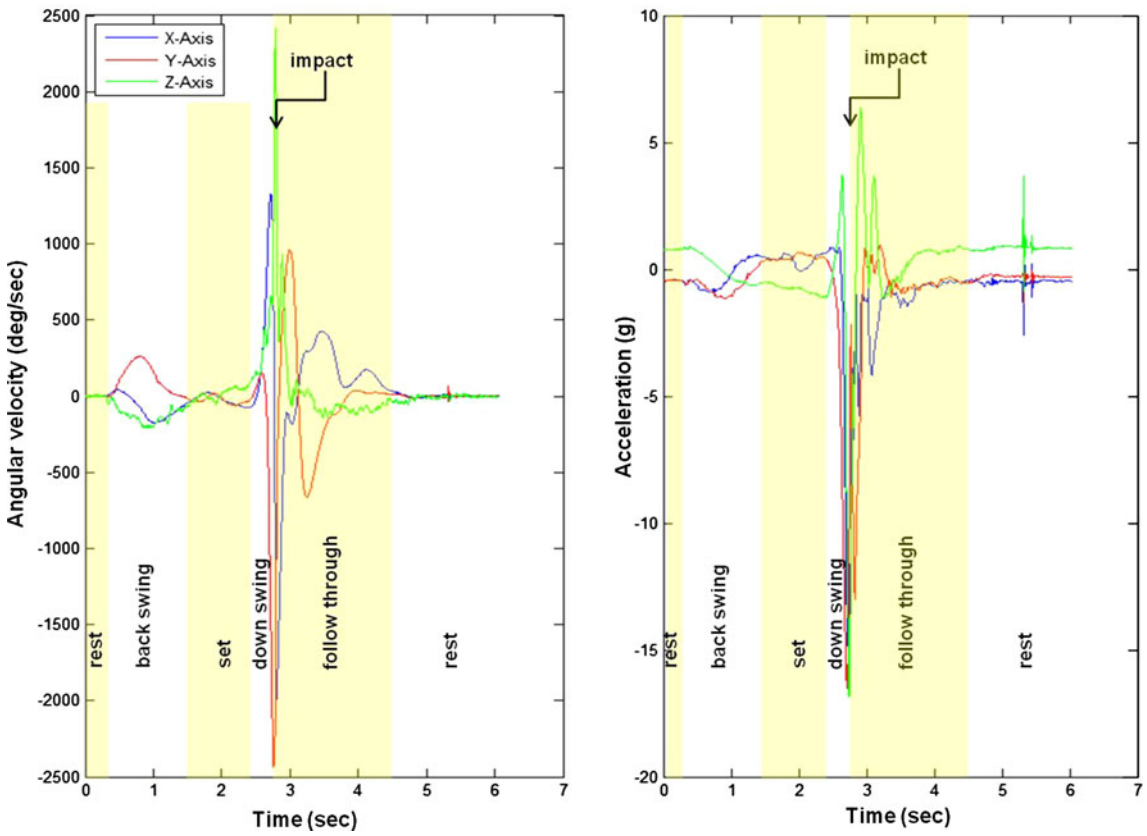


**Fig. 6** Components of angular velocity vector $(\omega_x, \omega_y, \omega_z)$ and acceleration vector $(a_x, a_y, a_z)$ measured by affixed IMU for same example swing by subject A. Reported components are measured relative to the IMU-fixed frame and are low pass filtered with 100 Hz cut-off. The major phases of the bat motion are readily identifiable

(Eq. 2) to obtain the associated orientation of the bat, thereby enabling one to animate the complete (6 dof) motion of the bat. Doing so with real IMU data, however, also introduces errors that are well known in the inertial navigation literature [22, 23]. Principal among these error sources is drift (or bias) error that ultimately degrades the aforementioned computation of orientation, velocity, and position. In this application, one can estimate drift errors by exploiting known kinematical states during the swing. For instance, the bat is at rest and the end of the barrel is located at the origin of the field-fixed frame at the start of the swing and returns to this state at the end. Moreover, the location of the ball on the tee is also known relative to the field-fixed frame and, at impact, the barrel of the bat contacts the ball at/near the sweet spot "*s*". These known kinematic conditions can be exploited to reduce/identify drift error in arriving at the following animations of three-dimensional bat motion.

Figure 7 illustrates the bat motion for the previous example (subject A) as viewed in the horizontal plane from a top view perspective looking down onto the batter. The bat in the middle of the set phase (dark blue image), the downswing, at impact (red image), and during the follow through are notated. These images are constructed every 10 ms with the exception of the ten (dark) images surrounding impact which are constructed every millisecond. This 10 ms period centered about impact is denoted as the "hitting zone" in which the bat remains in a well-defined "swing plane" (see below) just prior to, during and just after ball impact. The bat is also half toned (maize and blue) to enable one to visualize the roll of the bat during the swing as described above. This view clearly reveals the bat aim angle (Eq. 19) which is negative (−20.9°) in this example indicating the struck ball will pass to the right side of the pitcher's mound as viewed from the batter's box. This same view also reveals the trajectory of the knob/grip of the bat, which typically appears as two distinct spiral paths, one for the downswing and one for the follow through, that are joined at the impact position. The path of the grip (equivalent to the path of the batter's hands) may be of particular interest in coaching and assessing batter skill. For instance, batting coaches often state that faster bat speed is developed by keeping the hands close to the batter's body. By contrast, casting the bat far from the body increases the moment of inertia of the bat about the instantaneous axis of rotation yielding lower bat angular acceleration, angular velocity, and linear velocity. Thus, the geometry of the grip path may well serve as an important indicator of swing skill.

A view in the vertical plane and from the catcher's perspective provides valuable insight into the mechanics of the swing as shown in Fig. 8. Note the motion of the bat from the set through the downswing converges to a distinct bat "swing plane" in the hitting zone. This swing plane is defined by the elevation angle, which is −17.8° in this example. When hitting from a tee, the elevation angle is largely determined by the height of the batter and tee.

The oblique views illustrated in Fig. 9a, b are taken from the perspective of the batter's box facing the batter. This view allows visualization of the upper cut (or chop) angle (Eq. 17). Again, the upper cut angle defines the angle formed between the velocity vector of the sweet spot and

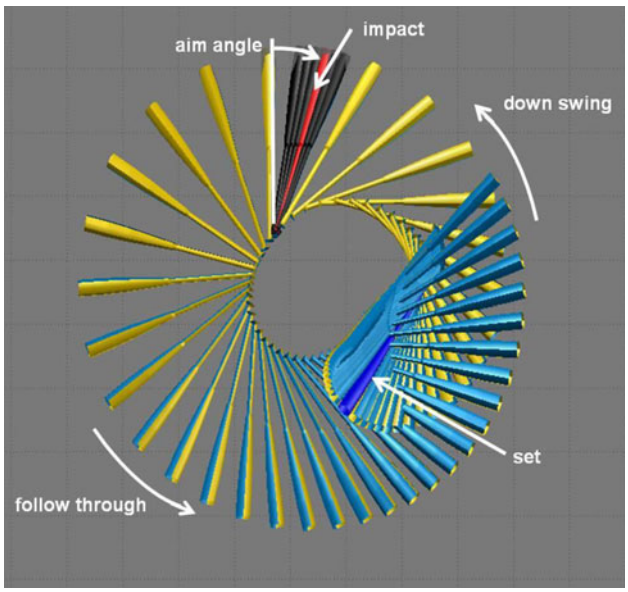


**Fig. 7** Top view of same bat swing (subject A) showing set, downswing, impact, and follow through phases of the swing. The bat aim angle at impact is noted

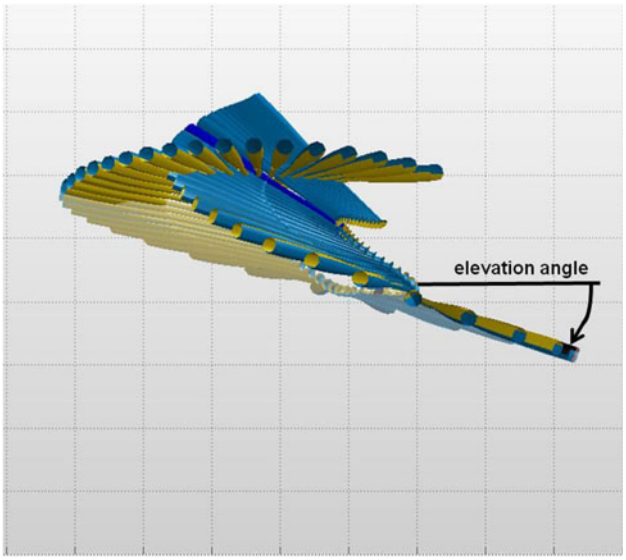


**Fig. 8** Catcher's view of same swing (subject A) depicting swing plane and elevation angle

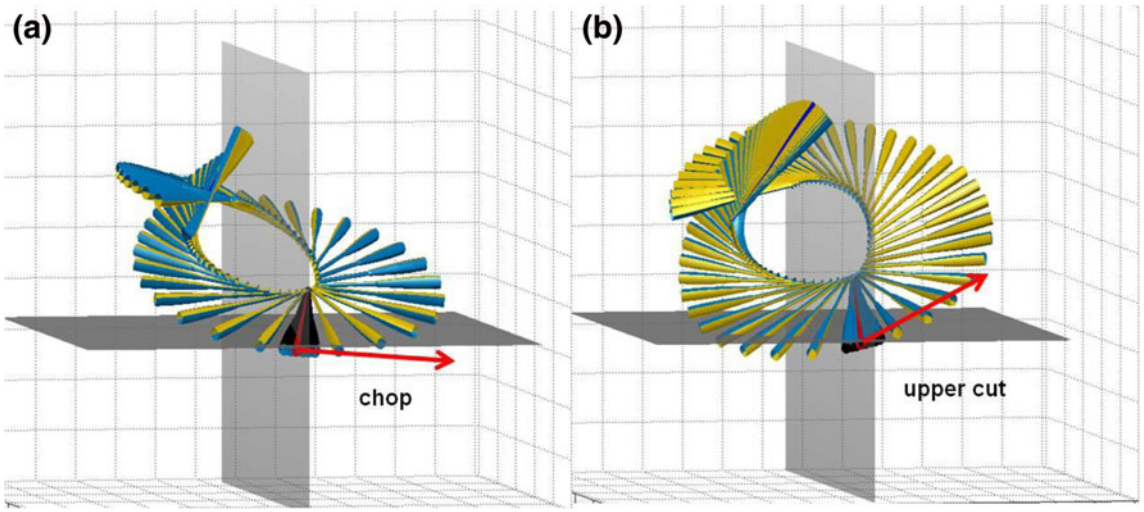


**Fig. 9** The oblique view of **a** same swing from subject A, and **b** example swing from subject B. View is taken from the perspective of the batter's box facing the batter. The swing for subject A illustrates a very modest chop whereas that for subject B illustrates a sizeable upper cut

the horizontal plane. Thus, when this angle is positive, as in Fig. 9b, the sweet spot is rising in the hitting zone representing an upper cut (of 12.2° in this example from subject B). By contrast, should this angle be negative, as in Fig. 9a, the sweet spot is falling in the hitting zone representing a chop (of a mere −3.9° in the continuing analysis of the example swing from subject A). The ability to identify and to precisely quantify the degree of upper cut or chop in a swing provides tremendous feedback to the player or coach who is often seeking a "level" swing.

In total, the aim, elevation and upper cut (or chop) angles defined above represent three obvious "swing metrics" that can be used to assess batting skill. Other candidate swing metrics follow from a quantitative analysis of critical timing, velocity and acceleration events as described next.

### 3.3 Analysis reveals critical timing, velocity and acceleration events

A batter's reaction to a pitched ball may be measured, in part, by how quickly the bat executes the downswing from the set position to ball impact. This "swing time" is readily observable in Fig. 10a, which illustrates the velocity of the grip (e.g. point "a" in Fig. 3) for the example swing for subject A. At the set position, the velocity components are approximately zero and the down swing begins when the grip speed $|\vec{v}_s|$ exceeds some threshold (selected here to be 1 m/s). Using this definition, the short duration swing time in this example is 165 ms. Within this brief period, the grip is accelerated from rest and achieves its maximum acceleration 249 m/s$^2$ at 149 ms into the downswing (i.e., 16 ms prior to impact) as illustrated in Fig. 10b. The associated velocity of the sweet spot achieves its maximum of 31.6 m/s (70.7 mph) essentially simultaneous with impact in this example. These timing events and the associated acceleration and velocity extrema are additional "swing metrics" that likely can be used to distinguish batter skill.

Immediately prior to and/or after impact, the batter must also impart significant roll to the bat to initiate and then complete the subsequent follow through phase of the swing. As introduced above, the bat roll angle measures rotation about the bat center-line axis. Figure 11 reports the bat roll angle and roll angular velocity as functions of time throughout the example swing for subject A. The bat is first "rolled" slowly during the backswing with little to no roll rate at the set position; then rolled quickly (and in the opposite sense) during the downswing and subsequent follow through. In this example, the maximum roll rate (2,136°/s) occurs just after impact (38 ms) and initiates the follow through phase. The maximum roll rate is achieved when the batter "breaks" her/his wrists enabling the hands to roll about the bat axis. This clearly observable "wrist break" and its delay past impact may well serve as another indicator of batter skill. Moreover, the roll of the bat is also a component of the bat motion that is extremely challenging to detect with any other technology.

### 3.4 Comments on accuracy

The IMU provides angular velocity and acceleration data, which are used to deduce a large number of kinematical quantities using the measurement theory of Sect. 2.2. The accuracy of these IMU-derived kinematical quantities may be assessed using a variety of methods. For example, in the context of the putting stroke used in golf, King et al. [13] demonstrate that IMU technology yields the orientation of

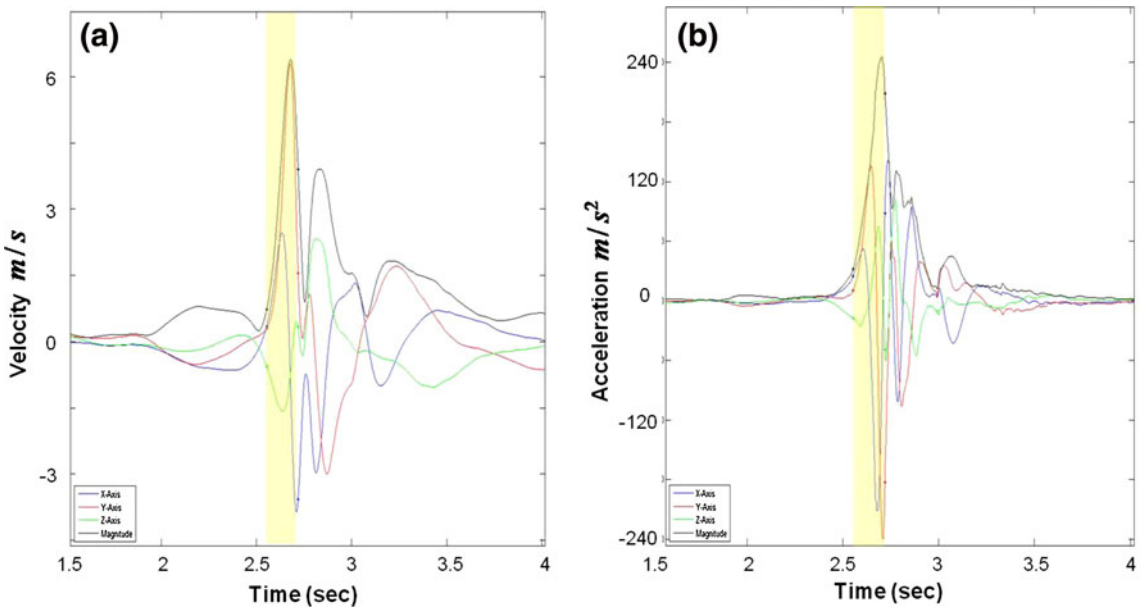


**Fig. 10** Velocity (**a**) and acceleration (**b**) of grip for example swing for subject A. All three components as well as the magnitude are reported as functions of time. The short time interval from the start of the down swing to ball impact is highlighted by the *shaded region*

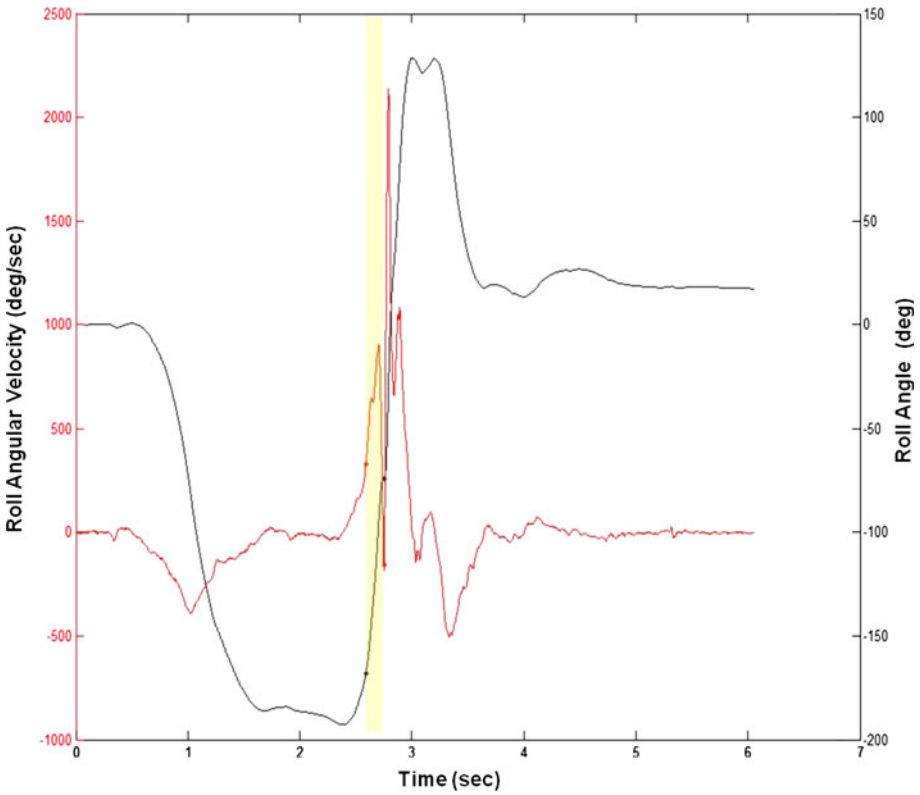


**Fig. 11** Bat roll rate (*red*) and roll angle (*black*) during the example swing for subject A. The short time interval from the start of the down swing to ball impact is highlighted by the *shaded region*

the club head (lie, loft and face angles) to within ±0.5° when benchmarked against a putting robot equipped with optical encoders (with angular resolution of ±0.07°). In addition, the position of the club head was shown to be accurate to within ±3 mm. In the context of bowling, the speed of the bowling ball center, as deduced from a ball-embedded IMU, remained within 3% of that measured directly using a radar gun [15].

In the context of swinging a bat, a key kinematical quantity is the velocity of the sweet spot since it strongly

**Fig. 12** Instrumented bat used for benchmarking study. Five reflective markers (four of which are visible in this image) were used with VICON motion analysis system to determine the velocity of the sweet spot. The knob-mounted IMU was used simultaneously to determine the velocity of the sweet spot

influences bat-ball impact. The accuracy of the IMU-derived sweet spot velocity was assessed herein using high-speed video motion capture as an independent benchmark. A 10-camera motion analysis system (VICON) was employed and calibrated such that marker errors for all ten cameras were less than 0.25 mm. Five reflective markers were affixed to the bat, four of which are visible in the image shown in Fig. 12. The 3D positions of these markers were measured by the VICON system using a sampling frequency of 240 Hz. The marker position data was used to determine the 3D position of the sweet spot (by interpolation of marker positions) and the sweet spot velocity was calculated by differentiation of this position data. The bat was also instrumented with an IMU for simultaneous recording of IMU data during a swing. A single subject was used for five trials. Following each trial, the velocity of the sweet spot at impact was deduced from the IMU and the VICON data and then used to calculate the percent difference in the sweet spot speed per

$$\%\ \text{difference} = \left| \frac{|\vec{v}_{s-\text{vicon}}| - |\vec{v}_{s-\text{imu}}|}{|\vec{v}_{s-\text{vicon}}|} \right| \times 100 \qquad (20)$$

The percent differences ranged from 5.7 to 9% with an average of 8.1% over the five trials. Note that, while these percent differences are small, they ultimately derive from modest inaccuracies inherent in *both* measurement technologies. For instance, the VICON-derived sweet spot velocity relies on differentiation of sampled position data with finite resolution of both position and time.

## 4 Summary and conclusions

This paper introduces a novel technology for bat swing analysis that is inexpensive and can be used right on the field of play for batter training and coaching. Additional potential uses include player rehabilitation and player-bat fitting. The technology exploits a highly miniaturized, wireless MEMS IMU affixed to the knob of the bat. The IMU incorporates three-axis sensing of bat acceleration and angular velocity with a low-power RF transceiver to transmit this data to a host computer. A companion measurement theory is summarized for integrating the acceleration and angular velocity data in reconstructing three-dimensional bat orientation, position, and velocity. Analysis of the raw and integrated data yields a large array of "bat swing metrics" that quantitatively define and therefore discriminate batting skill.

Both the raw data (angular velocity and acceleration) as well as the computed bat orientation (elevation, aim and roll angles) reveal the major phases of bat motion including the backswing, the set position (with superimposed bat waggle), the highly dynamic downswing, and the follow through. Integrating the raw data enables one to reconstruct and animate the three-dimensional motion of the bat throughout the entire swing. Doing so reveals critical bat swing metrics that have obvious value for batter coaching/training. These include the three-dimensional path described by the knob end of the bat (player's hands), the bat aim and elevation angles at impact, the swing plane in the hitting zone, and the degree of upper cut or chop at impact. Examination of the acceleration and velocity of the grip and the sweet spot reveal critical timing events that further quantify the swing. These include the swing time (which may also serve to measure batter reaction time), the time to maximum grip acceleration, the time between maximum bat speed and impact, and the time when the player "breaks" his/her wrists following impact.

Collectively, the measurement technology and the associated theory provide completely new capabilities for the sports of baseball and softball. Moreover, the same approach can be extended and specialized for a broad range of sports as disclosed in [16, 17].

**Acknowledgments** Ryan McGinnis gratefully acknowledges research support from the National Science Foundation through a Graduate Research Fellowship. Photographs courtesy of Lon Horwedel Photography. The authors also thank Dr. Scott McLean (Kinesiology, University of Michigan) for access to use his VICON motion analysis system.

**Conflict of interest** The authors declare that they have no conflict of interest.

## References

1. Welch CM, Banks SA, Cook FF, Draovitch P (1995) Hitting a baseball: a biomechanical description. J Orthop Sports Phys Ther 22(5):193–201

2. Nathan AM (2000) Dynamics of the baseball-bat collision. Am J Phys 68(11):979–990
3. Nicholls RL, Miller K, Elliot BC (2005) Numerical analysis of maximal bat performance in baseball. J Biomech 39(6):1001–1009
4. Smith L, Axtell JT (2003) Mechanical testing of baseball bats. J Testing Evaluat 31(3):210–214
5. Crisco JJ, Greenwald RM, Blume JD, Penna LH (2002) Batting performance of wood and metal baseball bats. Am Coll Sports Med 34(10):1675–1684
6. Brody H (1990) Models of baseball bats. Am J Phys 58(8): 756–758
7. Sawicki GS, Hubbard M, Stronge WJ (2003) How to hit home runs: optimum baseball bat swing parameters for maximum range trajectories. Am J Phys 71(11):1152–1162
8. Cross R (2005) A double pendulum swing experiment: in search of a better bat. Am J Phys 73(1):330–339
9. Koenig K, Mitchell ND, Hannigan TE, Clutter JK (2004) The influence of moment of inertia on baseball/softball bat swing speed. Sports Eng 7(2):105–117
10. Cross R (2009) Mechanics of swinging a bat. Am J Phys 77(1):36–43
11. Shapiro R (1979) Three-dimensional kinetic analysis of the baseball swing PhD Dissertation. University of Illinois at Urbana-Champaign, Urbana-Champaign
12. King KW, Yoon SW, Perkins NC, Najafi K (2004) The dynamics of the golf swing as measured by strapdown inertial sensors. In: Proceedings 5th International Conference on the Engineering of Sport, Davis, CA, USA, vol 2, pp 276–282
13. King KW, Yoon SW, Perkins NC, Najafi K (2008) Wireless MEMS inertial sensor system for golf swing dynamics. Sens Actuators A Phys 141:619–630
14. King KW, Perkins NC (2008) Putting stroke analysis using wireless MEMS inertia sensor systems. In: Proceedings World Scientific Congress on Golf V, Phoenix, AZ, USA, pp 270–278
15. King KW, Perkins NC, Churchill H, McGinnis R, Doss R, Hickland R (2011) Bowling ball dynamics revealed by miniature wireless MEMS inertial measurement unit. Sports Eng 13(2):95–104
16. Perkins NC (2006) Electronic measurement of the motion of a moving body of sports equipment. US Patent No. 7,021,140
17. Perkins NC (2007) Electronic measurement of the motion of a moving body of sports equipment. US Patent No. 7,234,351
18. King KW (2008) The design and application of wireless MEMS inertial measurement units for the measurement and analysis of golf swings. PhD Dissertation, University of Michigan
19. Goldstein H (1981) Classical Mechanics, 2nd edn. Addison-Wesley, White Plains, p 153
20. Haug EJ (1992) Intermediate dynamics. Prentice Hall, Upper Saddle River, pp 200–205
21. Kane TR, Likins PW, Levinson DA (1983) Spacecraft dynamics. McGraw-Hill, New York, pp 58–59
22. Savage PG (2002) Strapdown Analytics. Strapdown Associates, Inc., Maple Plane, pp 18.77–18.103
23. Rogers RM (2003) Applied mathematics in integration navigation systems. American Institute of Aeronautics and Astronautics, pp 163–178